International Journal of Mechanical, Industrial and Aerospace Sciences
ISSN: 2517-9950
Vol:7, No:6, 2013

Analytical and Finite Element Analysis of Hydroforming Deep Drawing Process

Maziar Ramezani and Thomas Neitzert

***Abstract*—**This paper gives an overview of a deep drawing process by pressurized liquid medium separated from the sheet by a rubber diaphragm. Hydroforming deep drawing processing of sheet metal parts provides a number of advantages over conventional techniques. It generally increases the depth to diameter ratio possible in cup drawing and minimizes the thickness variation of the drawn cup. To explore the deformation mechanism, analytical and numerical simulations are used for analyzing the drawing process of an AA6061-T4 blank. The effects of key process parameters such as coefficient of friction, initial thickness of the blank and radius between cup wall and flange are investigated analytically and numerically. The simulated results were in good agreement with the results of the analytical model. According to finite element simulations, the hydroforming deep drawing method provides a more uniform thickness distribution compared to conventional deep drawing and decreases the risk of tearing during the process.

***Keywords*—**Deep drawing, Hydroforming, Rubber diaphragm.

I. Introduction

MANY innovative deep drawing techniques have been introduced in recent decades to eliminate some problems of conventional deep drawing processes [1], [2]. The main purposes of these processes are enhancing the limiting drawing ratio, minimizing the variation of thickness of drawn cups, and reducing the cost of tooling especially for irregularly shaped parts. A class of these processes uses hydraulic pressure instead of one half metallic tool to increase the limiting drawing ratio and decrease the variation of thickness of the formed component. A higher depth to diameter ratio can be achieved by the hydroforming deep drawing process and irregular and unsymmetrical shapes can be drawn.

Fig. 1 shows the main components of the instrument for hydroforming deep drawing. It consists of a pressure container, a metallic rigid punch, blank-holder and a rubber membrane that is used for sealing the pressurized liquid in the container. The process starts by positioning the blank over the rubber diaphragm. The blank-holder is then positioned on top of the blank to prevent it from moving upward. A liquid is pumped into the cavity and at the last stage, the punch moves down to form the blank. The hydraulic pressure inside the container plays an important role throughout the drawing process. A pressure valve is generally used to control and regulate the liquid pressure inside the container. After the component is formed, the punch moves upward and the liquid in the container is withdrawn. The blank-holder can now be removed and the deep drawn cup can be collected from the press machine.

Because of the hydraulic pressure acting on the outer edge of the work-piece, a radial stress (equal to the fluid pressure) acts on the periphery of the flange. This radial stress helps to draw cups with higher drawing ratio before the cup wall reaches its ultimate tensile strength. The pressurized rubber pushes the cup to the punch and creates a frictional force between the blank and the punch contact area. This frictional stress helps to transfer the region of the maximum draw stress from the punch nose radius to the die radius, during the process. The limiting drawing ratio may also increases because of the absence of friction at the die radius which happens in the conventional deep drawing process. Thus, the combination of the radial stress in the periphery of the flange area and frictional stress in the cup wall, together with the absence of contact in the die radius region cause the higher drawing ratio achievable in hydroforming deep drawing. In this process, the radius at the intersection between the flange and the cup wall is not constant as there is no die present. The size of this radius can be controlled by changing the pressure inside the container and cups with small radius joining the flange area can be fabricated by increasing the pressure at the final stage. Since the blank is in contact with the rubber diaphragm instead of a rigid die, cups with very small radius between the wall and flange area can be produced without fracture. This is because of the hydraulic pressure pushing the rubber to the blank when it forms around the punch and the radial stress acting on the periphery of the flange. The combinations of these two stresses decrease the tension on the cup wall and postpone failure of the cup. However, if the hydraulic pressure is too high, it increases the frictional resistance between the blank and the blank-holder which will increase the drawing force necessary to form the cup causing the cup to fracture. On the other hand, if the pressure is too low, wrinkling will occur in the flange area. Because of the absence of a rigid die in this process, puckering may also occur at the connecting region between the flange and cup wall due to the lack of sufficient pressure. So, the pressure in the container should be regulated in such a way to keep a balance between these opposing effects [2].

For all the reasons mentioned above, deep drawing using hydroforming technique is considered to be the simplest

M. Ramezani is a Research Fellow at Centre of Advanced Manufacturing Technologies (CAMTEC), Auckland University of Technology, New Zealand. (Corresponding author, e-mail: mzramezani@gmail.com).

T. Neitzert is a Professor and director of Engineering Research Institute (ERI), Auckland University of Technology, New Zealand.

technique for producing complex shapes economically. It is also possible with this process, to draw complex parts in a single step, while it may requires several drawing steps and subsequent works if forming by the conventional deep drawing process. Other advantages include higher accuracy and dimensional control and better surface finish with scratch free drawn parts on one side.

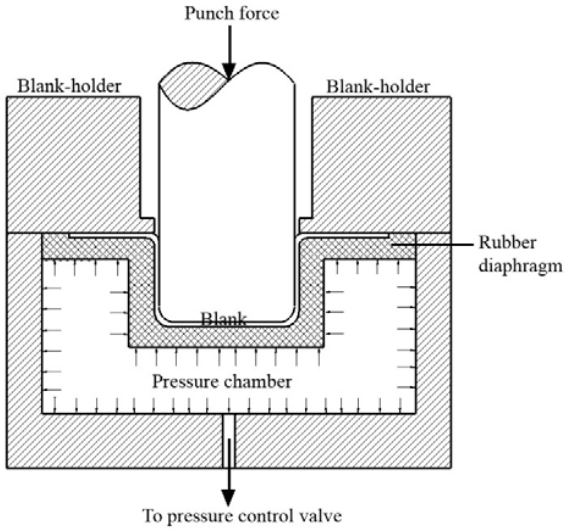

Fig. 1 Hydroforming deep drawing process

In a pioneering study, Fukui et al. [3] presented a mathematical analysis of the hydroforming deep drawing process based on total strain theory. They investigated the general characteristics starting from the use of fluid pressure as a die. Yossifon and Tirosh [4] developed a mathematical model for the hydroforming deep drawing process which provides the permissible operating fluid pressure path to avoid failure of the part. They showed that wrinkling and rupture of the work-piece can be avoided if the fluid pressure path can be restricted to travel only within their suggested bounds.

Thiruvarudchelvan and Lewis [5] designed and developed simplified tooling for a hydroforming deep drawing process that uses a constant hydraulic pressure. The experimental results and a simple theoretical analysis for the upper and lower bounds for the fluid pressure are presented in their article. In another study, Thiruvarudchelvan and Travis [1] investigated different versions of hydraulic-pressure-enhanced deep drawing processes and their advantages and disadvantages. Various aspects including the principles underlying these techniques are discussed in their paper.

Vollertsen et al. [6] introduced a deep drawing technique using multiple elastomer membranes pressurized by fluid media. They determined the necessary punch force for this process using a theoretical model. Kandil [7] investigated the hydroforming deep drawing of aluminum and copper blanks experimentally. He studied the effect of main process parameters such as the initial pressure, sheet thickness, sheet material properties, punch geometry, punch load and drawing ratio on the drawing performance of the cup.

Lang et al. [8], [9] presented a new hydro-mechanical deep drawing technique assisted by radial pressure. In this method, a radial pressure is loaded along the blank rim to reduce the drawing force. They used experimental and finite element approaches for analyzing the forming process of aluminum alloy blanks. Djavanroodi and Derogar [10] investigated the formability, fracture mode and strain distribution of aluminum and titanium alloy sheets during the hydroforming deep drawing process. They also studied the effect of process parameters on forming limit diagram by using finite element simulations.

In the present paper an analytical analysis has been carried out to study the effect of the process parameters on the hydroforming deep drawing process. It is followed by finite element simulations of the process to investigate the deformation mechanism of the drawn cups. The relationship between the deep drawing ratio, blank thickness, drawing pressure, and drawing load during hydroforming operation are presented. Comparisons between the results of the analytical model and the results obtained by finite element simulations are also carried out.

II. Theoretical Analysis

A. Conventional Deep Drawing of Cylindrical Cups

Considering the deformation of a flange during cylindrical cup drawing, two major deformation mechanisms are often found in deep drawing: (1) biaxial stretching over the punch, in which both principal strains in radial and hoop directions are tensile, and (2) drawing the flange into the die cavity in which the radial principal strain is tensile and the hoop principal strain is compressive.

During a deep drawing process, the flange area of the blank is subjected to a combination of a radial tensile stress and an induced compressive hoop stress. Wrinkles may occur in the flange portion if the magnitudes of these two stresses reach a critical value. This critical value mostly depends on the current flange dimensions and the properties of the blank material. To prevent or postpone wrinkling in the flange area, blank-holders are usually used.

Several analytical models are available for the conventional deep drawing process [11], [12]. In all of these models, two major regions are considered for the mathematical modeling of deep drawing, i.e. the flange area and the cup wall. The wall of the drawn cup undergoes a considerable drawing force to cause the deformation in the flange. For blanks with a large diameter, the necessary drawing force acting on the wall to draw the blank through the die might go beyond the ultimate tensile stress of the material and will cause necking or fracture in the cup. The formability in deep drawing is usually characterized by limiting drawing ratio (LDR) of the cup, which can be described as the ratio of the largest diameter of the blank that can be drawn without failure, to the diameter of the punch [13]. The theory described here for conventional deep drawing is from the work of Mielnik [13]. He made the following simplified assumptions for the analytical modeling:

1. The work due to external and internal friction loss due to bending and unbending is initially neglected and it will be

considered at the final step by employing a deformation efficiency factor η.

2. Since the strain-hardening exponent n has negligible effect on limiting drawing ratio (LDR), the material of the work-piece is considered to be perfectly plastic with $n = 0$.
3. The thickness of the sheet remains constant during the drawing process.
4. The material has planar isotropy.

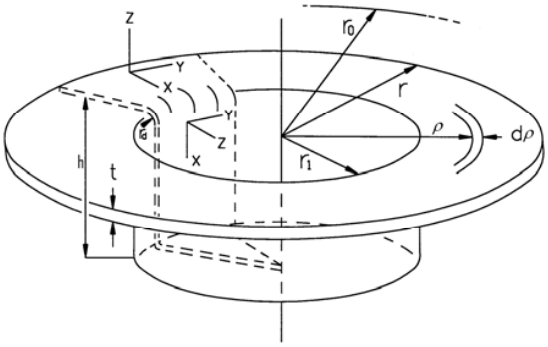

Fig. 2 Schematic illustration of a partially drawn cup showing the dimensional notation

The deformation mechanism in the flange during the deep drawing process is shown in Fig. 2. Assuming the plane strain condition in the flange ($\varepsilon_z = 0$), volume constancy of the sheet leads to the following relationship:

$$\pi \rho_0^2 = \pi \rho^2 + 2\pi r_1 h = \text{constant} \tag{1}$$

where ρ_0, ρ, r_1 and h are illustrated in Fig. 2. By taking the derivative, we arrive at:

$$2\pi \rho \, d\rho + 2\pi r_1 dh = 0 \quad \text{or} \quad d\rho = -\frac{r_1 \, dh}{\rho} \tag{2}$$

Considering $d\varepsilon_y = \dfrac{d\rho}{\rho}$ and $d\varepsilon_z = 0$, we have:

$$d\varepsilon_x = -d\varepsilon_y = -\frac{d\rho}{\rho} = \frac{r_1 \, dh}{\rho^2} \tag{3}$$

where r_1 is the cup radius and dh is the incremental punch travel. The incremental work dW done on the element shown in Fig. 2 is equal to the volume of the element $2\pi t \rho \, d\rho$ times the incremental work per volume $\sigma_x d\varepsilon_x + \sigma_y d\varepsilon_y + \sigma_z d\varepsilon_z$. Since $d\varepsilon_z = 0$ and $d\varepsilon_x = -d\varepsilon_y$, the work per volume is $(\sigma_x - \sigma_y)\sigma \, d\varepsilon_x$, and so the work on this element is:

$$dW = \frac{2\pi t \, \rho \, d\rho \, (\sigma_x - \sigma_y)(r_1 \, dh)}{\rho^2} \tag{4}$$

The total work for an ideally plastic material on all elements of the flange per increment of punch travel is:

$$\frac{dW}{dh} = \int_{r_1}^{r} \frac{2\pi r_1 t \sigma_f}{\rho} d\rho = 2\pi r_1 t \sigma_f \ln\left(\frac{r}{r_1}\right) = F_d \tag{5}$$

The drawing force F_d, is maximum at the beginning of the draw, when $r = r_0$, so:

$$F_{d\max} = 2\pi r_1 t \sigma_f \ln\left(\frac{r_0}{r_1}\right) = 2\pi r_1 t \sigma_f \ln\left(\frac{d_0}{d_1}\right) \tag{6}$$

$$\sigma_{d\max} = \sigma_f \ln\left(\frac{d_0}{d_1}\right) \tag{7}$$

where d_0 and d_1 are the blank and cup diameters, respectively, σ_d is the drawing stress and σ_f is the flow stress of the sheet in the flange. This equation is valid for 100 percent deformation efficiency, i.e., for $\eta = 1$. By taking into account the external and internal frictions, the deformation efficiency factor (η) can be introduced into (7). Therefore, at any instant as the cup is being drawn at d_i, the drawing stress for a deformation efficiency of η can be given by:

$$F_d = \frac{1}{\eta} \pi d_i t \sigma_f \ln\left(\frac{d_i}{d_1}\right) \tag{8}$$

$$\sigma_d = \frac{1}{\eta} \sigma_f \ln\left(\frac{d_i}{d_1}\right) \tag{9}$$

Let us now consider the deformation mechanism in the cup wall. To avoid failure, the cross-sectional area of the cup wall must withstand the maximum drawing force $F_{d\max}$. So, the limiting drawing ratio will be reached when the axial stress σ_x reaches the flow stress of the sheet in the wall σ_w.

$$\sigma_x = \sigma_w = \frac{F_{d\max}}{2\pi r_1 t} = \sigma_f \ln\left(\frac{d_0}{d_1}\right) \tag{10}$$

Therefore, the wall of the cup will begin to neck when $\sigma_x = \sigma_w$. Since the circumference of the wall is constrained by the rigid punch from shrinkage, plane strain occurs, where $\varepsilon_y = 0$, and so the limiting drawing ratio ($\mathrm{LDR} = \frac{d_{0\max}}{d_1}$) can be obtained by the ratio of the two plane-strain flow strengths, that is, σ_w of the cup wall and σ_f of the flange, as follows:

$$\frac{\sigma_w\ (\varepsilon_y = 0)}{\sigma_f\ (\varepsilon_z = 0)} = \ln(LDR) \tag{11}$$

For the isotropic case and for an ideally plastic material, $\sigma_f = \sigma_w$, (11) leads to $\mathrm{LDR} = \exp(1) = 2.72$. However, compared to practical results, this is too high and hence, the calculated work in the flange and the calculated drawing force should be modified by multiplying with the deformation efficiency factor, η to take into account the work against friction and the work to cause bending. In this case $\mathrm{LDR} = \exp(\eta)$. Usually the LDR is about 2, and so the efficiency is roughly 0.70.

B. Hydroforming Deep Drawing of Cylindrical Cups

The analytical model presented in this section is based on the work of Fukui et al. [3]. The mathematical analysis for deep drawing using hydroforming is fundamentally the same as conventional deep drawing analysis and the only difference is the consideration of the effect of liquid pressure. The high pressure in the liquid chamber pushes the blank to the rigid tools and causes frictional resistance between blank-holder and flange portion of the blank (Fig. 3 A-B). At the other side of the blank which is in contact with the rubber diaphragm, the rubber deforms and moves with the blank and therefore, the frictional resistance at blank-rubber contact surface is not significant. Considering the blank-holder plate as a plane normal to the punch axis, the relations for radial stress and strain can be expressed as:

$$\frac{d(\sigma_x.R.t)}{dR} = \sigma_y\, t + \mu\, p_i\, R \tag{12}$$

$$\frac{d\varepsilon_y}{dR} = \frac{1}{R}(1 - e^{\varepsilon_y - \varepsilon_x}) \tag{13}$$

For the flange portion, we have from (12) and (13):

$$A = R + R\sigma_x[\frac{1}{4}Km(\bar{\sigma})^{m-2}(2\sigma_z - \sigma_x - \sigma_y)\times(2\sigma_x - \sigma_y - \sigma_z) - \frac{1}{2}K(\bar{\sigma})^m]$$

$$B = R\sigma_x[\frac{1}{4}Km(\bar{\sigma})^{m-2}(2\sigma_z - \sigma_x - \sigma_y)\times(2\sigma_y - \sigma_x - \sigma_z) - \frac{1}{2}K(\bar{\sigma})^m]$$

$$C = \sigma_y - \sigma_x + \mu\, p\frac{R}{t}$$

For conventional deep drawing processes, the second term in the right hand side of (12) becomes zero since $p_i = 0$. Similarly, the relation for radial stress and strain in the forming radius portion (Fig. 3 B-C) is given as:

$$\frac{d(\sigma_x.R.t)}{dR} = \sigma_y\, t \tag{14}$$

$$\frac{d\varepsilon_y}{dR} = \frac{1}{R}(1 - \frac{1}{\sin\theta}e^{\varepsilon_y - \varepsilon_x}) \tag{15}$$

For conventional deep drawing processes, a term caused by friction would be added to the right hand side of (14). However, for the case of hydroforming, the friction between rubber and blank can be neglected.

In the preceding equations, σ represents true stress and ε represents logarithmic strain. As shown in Fig. 2, the subscripts *x*, *y* and *z* represent the radial, circumferential and thicknesswise components, respectively. Considering the relationship between equivalent stress $\bar{\sigma}$ and equivalent strain $\bar{\varepsilon}$ as $\bar{\sigma} = c(\bar{\varepsilon})^n$, the general relation between stress and strain in the plastic range can be given as follows:

$$\begin{aligned}
\varepsilon_x &= K(\bar{\sigma})^m(\sigma_x - \frac{\sigma_y + \sigma_z}{2}) \\
\varepsilon_y &= K(\bar{\sigma})^m(\sigma_y - \frac{\sigma_x + \sigma_z}{2}) \\
\varepsilon_z &= K(\bar{\sigma})^m(\sigma_z - \frac{\sigma_x + \sigma_y}{2})
\end{aligned} \tag{16}$$

where $K = (1/c)^{(1/n)}$ and $m = (1-n)/n$ are material constants that can be determined from tensile tests. Combining (12), (13), (14), and (15) with (16), the following simultaneous equations can be established.

$$\begin{aligned}
\frac{d\sigma_x}{dR} &= \frac{B'C - BC'}{AB' - A'B} \\
\frac{d\sigma_y}{dR} &= \frac{AC' - A'C}{AB' - A'B}
\end{aligned} \tag{17}$$

$$A' = \frac{1}{4}Km(\bar{\sigma})^{m-2}(2\sigma_x - \sigma_y - \sigma_z)\times(2\sigma_y - \sigma_x - \sigma_z) - \frac{1}{2}K(\bar{\sigma})^m$$
$$B' = \frac{1}{4}Km(\bar{\sigma})^{m-2}(2\sigma_y - \sigma_x - \sigma_z) + K(\bar{\sigma})^m$$
$$C' = \frac{1}{R}\left[1 - \exp[\frac{3}{2}K(\bar{\sigma})^m(\sigma_y - \sigma_x)]\right]$$

For the forming radius portion and from (14) and (15), we have:

$$A = R + R\sigma_x[\frac{1}{4}Km(\bar{\sigma})^{m-2}(2\sigma_z - \sigma_x - \sigma_y)\times(2\sigma_x - \sigma_y - \sigma_z) - \frac{1}{2}K(\bar{\sigma})^m]$$
$$B = R\sigma_x[\frac{1}{4}Km(\bar{\sigma})^{m-2}(2\sigma_z - \sigma_x - \sigma_y)\times(2\sigma_y - \sigma_x - \sigma_z) - \frac{1}{2}K(\bar{\sigma})^m]$$
$$C = \sigma_y - \sigma_x$$
$$A' = \frac{1}{4}Km(\bar{\sigma})^{m-2}(2\sigma_x - \sigma_y - \sigma_z)\times(2\sigma_y - \sigma_x - \sigma_z) - \frac{1}{2}K(\bar{\sigma})^m$$
$$B' = \frac{1}{4}Km(\bar{\sigma})^{m-2}(2\sigma_y - \sigma_x - \sigma_z) + K(\bar{\sigma})^m$$
$$C' = \frac{1}{R}\left[1 - \frac{1}{\sin\theta}\exp[\frac{3}{2}K(\bar{\sigma})^m(\sigma_y - \sigma_x)]\right]$$

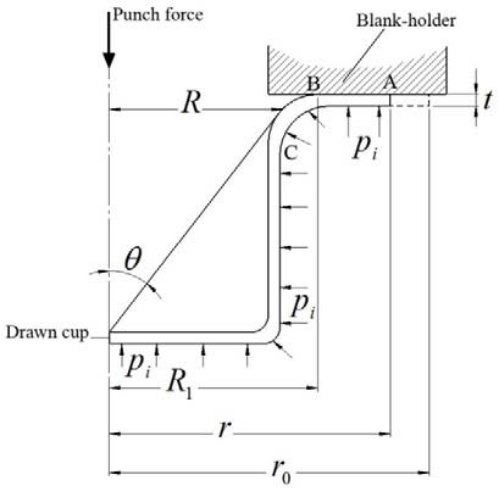

Fig. 3 Geometry of cup during deep drawing process

The above equations can be used to determine the stress and strain distributions in the formed component. To solve these equations numerically, the initial values of σ_{x0}, σ_{y0} and σ_{z0} for the flange portion can be found as follows:

$$R = r \quad \Rightarrow \quad \sigma_{x0} = \sigma_{z0} = p_i$$

So, from (16) we have:

$$\varepsilon_{y0} = \ln(\frac{r}{r_0}) - K(\sigma_{x0} - \sigma_{y0})^{m+1}$$

For forming radius portion, the initial values of σ_x and σ_y at point B (Fig. 3) on the inside edge of the flange are used. For this reason, the position of point B must be determined, since point B varies with the applied forming pressure and the value of the radial stress created in the blank piece. By taking the punch and the blank portion R_1, as shown in Fig. 3 as an integral unit and taking into account the axial equilibrium, we will have:

$$F_d = \pi R_1^2 \, p_i$$

In numerical calculations, the punch force F_d found from FE simulations were used for determining the value of R_1.

C. Drawing Stress

Drawing stress of the cup body at any instant of the hydroforming deep drawing process is given by [17]:

$$\sigma_d = \frac{F_d}{\pi d_p t} = \sigma_{id} + \sigma_{fric} + \sigma_b = 1.1\sigma_f \ln\beta - p_i + \frac{(\mu_m + \mu_b)p_i}{8}(\beta^2 - 1)(\frac{1}{\beta} + 1)\frac{d_p}{t} + \sigma_{fs}(\frac{t}{2r_d}) \quad (18)$$

where F_d is the force on the cup wall needed for drawing, d_p is the punch diameter, t is the original thickness of the

blank, β is the draw ratio, p_i is the internal fluid pressure in the die cavity, μ_m is the coefficient of friction between membrane and sheet metal, μ_b is the coefficient of friction between blank-holder and sheet metal, and r_d is the radius between cup wall and flange. $\sigma_b = \sigma_{fs}(\frac{t}{2r_d})$ is the stress caused by bending and unbending; σ_{fric} is the friction stress in the region of the flange; and $\sigma_{id} = 1.1\sigma_f \ln\beta - p_i$ is the ideal forming stress. σ_f is the average flow stress of sheet material in the flange region and is almost equal to $1.35\sigma_{ult}$, where σ_{ult} is the ultimate tensile strength of the sheet metal. σ_{fs} is the yield stress of the work-hardened material at the die-corner regions, and can be determined using the following relationship:

$$\sigma_{fs} = c\left(\ln\sqrt{1+\frac{t}{r_p}}\right)^n \tag{19}$$

where c and n are the strength coefficient and strain hardening exponent of the sheet metal, respectively, and r_p is the punch edge radius.

Under high internal pressure the blank is completely surrounded by the rubber diaphragm. Due to the incompressibility of rubber, it can be assumed to behave like a liquid and thus the internal pressure p_i acts on the flange area of the blank too and reduces the ideal drawing force. According to Panknin and Muhlhauser [17], the value of internal pressure p_i can be subtracted from (18). Subtracting p_i from equation of σ_{id} leads to:

$$\sigma_d = 1.1\sigma_f \ln\beta + \frac{(\mu_m+\mu_b)p_i}{8}\left[(\beta^2-1)(\frac{1}{\beta}+1)\frac{d_p}{t}\right] + \sigma_{fs}(\frac{t}{2r_d}) \tag{20}$$

which gives the drawing stress of the cup wall along the drawing direction. Using (18) and (20), the drawing force can be simply calculated as:

$$F_d = \pi d_p t[1.1\sigma_f \ln\beta + \frac{(\mu_m+\mu_b)p_i}{8}\times [(\beta^2-1)(\frac{1}{\beta}+1)\frac{d_p}{t}] + \sigma_{fs}(\frac{t}{2r_d})] \tag{21}$$

To prevent the blank from lifting off the blank-holder when the punch pushes on it, F_d must be less than the load applied on the annular area of the blank by the hydraulic pressure p_i [5]. Therefore, we must have:

$$F_d = \sigma_d \pi d_p t < p_i \frac{\pi}{4}(D^2 - d_p^2) \tag{22}$$

where D is the flange diameter. Simplifying (22) we arrive at:

$$\sigma_d < \frac{p_i}{4d_p t}(D^2 - d_p^2) \tag{23}$$

Furthermore, to prevent lifting off of the blank-holder during the hydroforming deep drawing process, the minimum pressure can be determined as follows by combining (20) and (23):

$$p_i > \frac{1.1\sigma_f \ln\beta + \sigma_{fs}(\frac{t}{2r_d})}{\frac{1}{4d_p t}(D^2-d_p^2) - \frac{(\mu_m+\mu_b)}{8}(\beta^2-1)(\frac{1}{\beta}+1)\frac{d_p}{t}} = \frac{1.1\sigma_f \ln\beta + \sigma_{fs}(\frac{t}{2r_d})}{\frac{d_p}{4t}(\beta^2-1) - \frac{(\mu_m+\mu_b)}{8}(\beta^2-1)(\frac{1}{\beta}+1)\frac{d_p}{t}} \tag{24}$$

However, to prevent wrinkling of the flange and puckering in the unsupported areas, the internal pressure would have different lower limits which were analyzed in [4].

On the other hand, to avoid instability of the cup wall in tension that leads to fracture, we must have $\sigma_d < \sigma_{ult}$. Using (20) we arrive at:

$$p_i < \frac{\sigma_{ult} - 1.1\sigma_f \ln\beta - \sigma_{fs}(\frac{t}{2r_d})}{\frac{(\mu_m+\mu_b)}{8}(\beta^2-1)(\frac{1}{\beta}+1)\frac{d_p}{t}} \tag{25}$$

In practice, to avoid excessive thinning of the cup wall, the draw stress is kept considerably below the ultimate tensile strength of blank material and thus, (25) gives an over-estimate of the hydraulic pressure. Therefore, from the simplified theoretical analysis presented above, the liquid

pressure, p_i in hydroforming deep drawing process must lie within the limits given by (24) and (25)

III. Finite Element Simulation

Finite element simulations have been used for analysis and design of metal working processes in recent years. Compared to experimental analysis, computer simulations have the advantages of low cost, short time, more information and well-illustrating graphics, although they require practical verification. The numerical simulations of the hydroforming deep drawing process were conducted in ABAQUS based on finite element formulation. The dimensions of the tools used in the simulations are listed in Table I. By taking advantage of axisymmetry it was possible to simulate the die, blank and rubber assembly as a 2-D axisymmetric model. Two different types of elements, namely CAX4R and CAX4RH, were employed to model the blank and the rubber, respectively. The Young's modulus and Poisson's ratio of the blank material were selected to be 70.4*GPa* and 0.33, respectively.

TABLE I
Dimensions of the Tools for FE Simulations

Parameters	Values
Punch diameter, d_p (mm)	70
Punch nose radius, r_p (mm)	5
Blank initial diameter, d_0 (mm)	160
Blank initial thickness, t (mm)	1.5
Rubber diaphragm thickness (mm)	10

TABLE II
Properties of AA6061-T4 [9]

Parameters	Values
Yielding stress, σ_{yield} (MPa)	125
Ultimate tensile stress, σ_{ult} (MPa)	227
Young's modulus, E (GPa)	70.4
Poisson's ratio, ν	0.33
Strain hardening exponent, n	0.236
Hardening coefficient, c (MPa)	405

A Coulomb friction law was assumed. The friction coefficient was equal to 0.1 between blank and metallic tools and 0.25 between blank and rubber diaphragm. The values of the coefficients of friction are based on the results of a friction analysis of a rubber-pad forming process conducted previously by one of the authors [14]. Surface to surface contact algorithm was selected to model the contact between the sheet metal and tools including punch, rubber diaphragm and blank-holder. The movement of the punch was defined using its reference node. This node was also employed to obtain the drawing force during the simulation. Appropriate boundary conditions were applied to the models of sheet, punch, rubber and blank-holder. The blank-holder was fully constrained and the punch could move only along the *Z*-direction, corresponding to the central axis of the punch. The punch motion used a constant velocity profile in order to limit inertial effects. All metallic tools were modeled as analytical rigid bodies. The blank and rubber were modeled as deformable bodies.

An elasto-plastic material model with Hill's yield criteria was used for the blank. The blank material is aluminum alloy 6061-T4. The mechanical properties of AA6061-T4 are listed in Table II. The strain-hardening model applied in the simulation was isotropic hardening, and the material characteristics were represented by the power law, which is given by:

$$\sigma = c\,\varepsilon^{n} \tag{26}$$

where σ is the flow stress (*MPa*), ε is the total true strain (dimensionless), c is the strength coefficient (*MPa*) and n is the strain-hardening exponent (dimensionless).

Flexible materials have nonlinear stress–strain characteristics for relatively large deformations. Under such conditions, they are generally assumed as nearly incompressible. To model these hyper-elastic materials through FEM, a constitutive law based on total strain energy density *W* has to be adopted. Among several approaches, Ogden theory [15] was used to model rubber material in finite element simulations. This material model has previously been used with success to predict the behavior of hyper-elastic materials [16]. The form of the Ogden strain energy potential is:

$$\sigma_{ij} = \frac{\partial W}{\partial \varepsilon_{ij}} \tag{27}$$

$$W = \sum_{i=1}^{N} \frac{2\mu_i}{\alpha_i^2}(\bar{\lambda}_1^{\alpha_i} + \bar{\lambda}_2^{\alpha_i} + \bar{\lambda}_3^{\alpha_i} - 3) + \sum_{i=1}^{N} \frac{1}{D_i}(J^{el} - 1)^{2i} \tag{28}$$

where *W* is the strain energy per unit of reference volume; $\bar{\lambda}_i$ are the deviatoric principal stretches which can be defined by $\bar{\lambda}_i = J^{\frac{-1}{3}}\lambda_i$; J is the total volume ratio; J^{el} is the elastic volume ratio; and μ_i, α_i and D_i are temperature-dependent Ogden constants. Compressibility can be defined by specifying nonzero values for D_i, by setting the Poisson's ratio to a value less than 0.5, or by providing test data that characterize the compressibility. We assumed a fully incompressible behavior for rubber with $\nu = 0.4997$ and D_i equal to zero and then, the second expression in (28) can be eliminated. To determine the strain energy density *W*, ABAQUS uses a least-squares fitting algorithm to evaluate the Ogden constants automatically from a stress-strain curve. The stress-strain curve of the polyurethane is presented in Fig. 4.

IV. Results and Discussions

The distribution of the von-Mises stress in the drawn cup at the last stage of the simulation is illustrated in Fig. 5. The maximum FE predicted von-Mises stress for the blank at the last step of the forming process is 259*MPa*. Fig. 6 shows the punch load-stroke curve for hydroforming deep drawing of a AA6061-T4 blank, obtained from FE simulation. As can be seen from the figure, the maximum load is 182.56kN at punch stroke of 48mm. The maximum load predicted using (21) is 194.30kN which shows a 6% error.

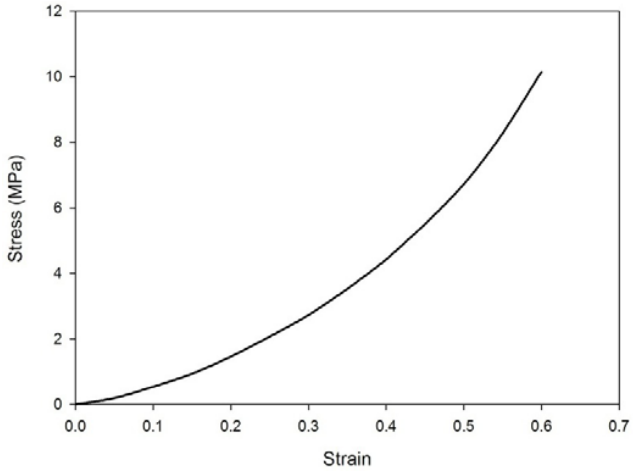

Fig. 4 Stress-strain diagram of polyurethane

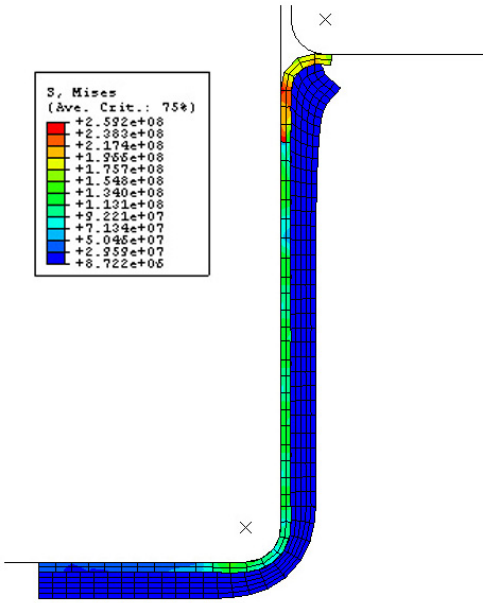

Fig. 5 Distribution of von-Mises stress at the final stage of hydroforming deep drawing

The distribution of von-Mises stress in the rubber diaphragm at the end of the process is shown in Fig. 7. As illustrated in the figure, the maximum von-Mises stress occurs at the punch nose region where it is forced to deform excessively together with the drawing of the blank. The regions of the rubber diaphragm which are in contact with the bottom of the cup have relatively same level of stress which causes the rubber to exert a quite uniform pressure to the blank. The maximum principal logarithmic strain of the rubber diaphragm at the end of the process is shown in Fig. 8. As can be seen in the figure, the regions of the flexible punch which are in contact with the blank, have the lowest strain which is because of the cohesive behavior of rubber. This behavior causes a stick region between rubber and blank and helps to form the part more uniformly. The maximum principal logarithmic strain happens at the middle of the rubber in punch nose region, where the punch pushes the blank to form and take the shape of the punch. Therefore, considering the strain behavior of rubber diaphragm, it should be designed such that its dimensional stability could be preserved during the process.

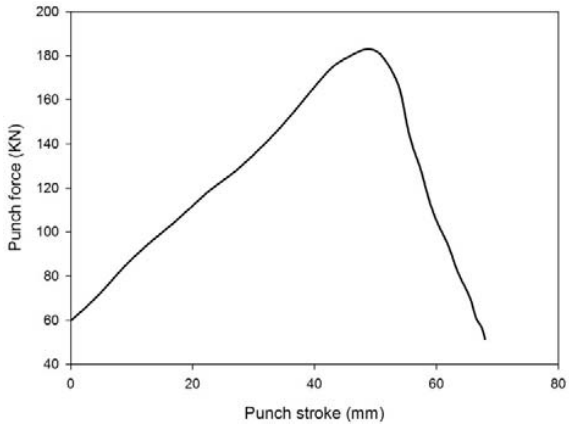

Fig. 6 Punch load-stroke curve for hydroforming deep drawing of AA6061-T4 obtained from FE simulation

Using the mathematical model presented in Section II. *B*, the distribution of stress and strain at zone A to C (see Fig. 3) of the blank is calculated. Figs. 9 and 10 show the true stress and logarithmic strain at the punch stroke of 25mm and Figs. 11 and 12 show the true stress and logarithmic strain distribution at the punch stroke of 50mm. According to the figures, a tensile radial stress develops in the blank during the hydroforming deep drawing process and the value of this tensile stress increases constantly from the periphery of the blank to the wall region. By comparison of Figs. 9 and 11, it can be also seen that the radial stress increases as the punch stroke increases. On the other hand, the model predicts a negative circumferential stress which is quite constant in the flange area of the blank. This compressive circumferential stress decreases as we move from the flange area to the cup wall area. According to the figures, the circumferential stress increases, as the punch stroke increases. The thicknesswise stress has a constant value throughout the process which is equal to the value of fluid pressure inside the chamber.

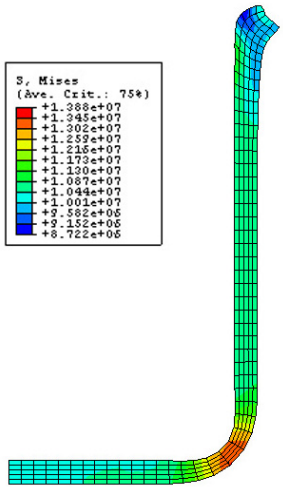

Fig. 7 Distribution of von-Mises stress in rubber diaphragm at the end of the process

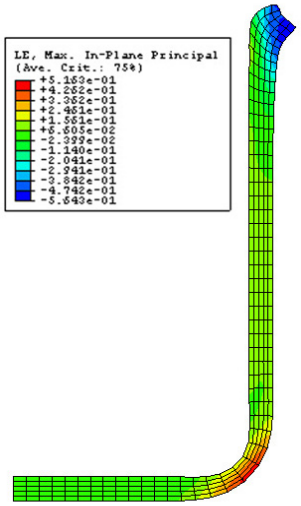

Fig. 8 Distribution of Logarithmic strain in rubber diaphragm at the end of the process

According to Figs. 10 and 12, the radial logarithmic strain is positive throughout the process. This is because of the descending of the punch which forces the blank to stretch and take up the shape of the punch into the cavity. As the punch stroke increases, the blank radial strain increases. The thicknesswise strain starts from a positive value and becomes negative at the bending area of the cup. This shows that the thickness increases slightly at the flange area and decreases at the bending area and wall of the cup. The circumferential strain has a negative value during the simulation. A comparison of Figs. 10 and 12 shows that the values of radial and circumferential strain reaches a maximum value at a punch stroke of 25mm and then decreases as we move to the cup wall area. However, as the punch stroke increases, the strain values increase constantly during the process at A to C zone and there is no decrease in the values.

To compare the results of the analytical model with the finite element simulation, the values of equivalent stress at points A to C (see Fig. 3) resulting from the two methods are compared for the punch stroke of 50mm. As illustrated in Fig. 13, the equivalent stress increases continuously and reaches its maximum value at point C. As can be seen in this figure, the values of equivalent stress obtained from both methods correlate with each other. In general, the finite element simulation method tends to predict the stress value higher than the analytical model at the flange area and lower than the analytical model at the bend radius area. The difference of predicting equivalent stress at point C using these two methods is 10.4%.

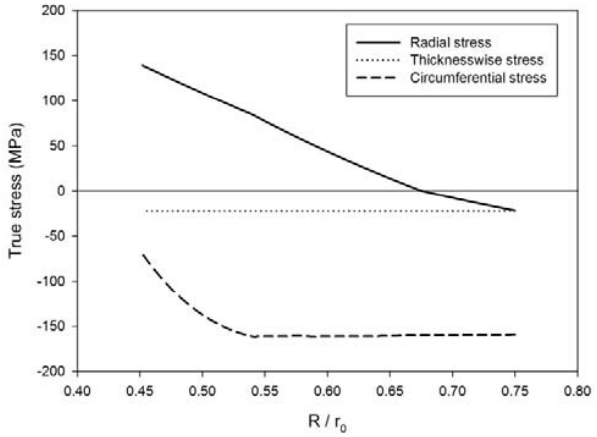

Fig. 9 Stress distribution in AA6061-T4 blank at the punch stroke of 25mm

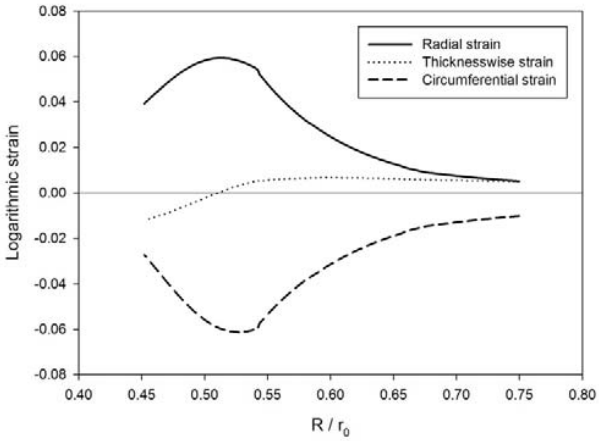

Fig. 10 Logarithmic strain in AA6061-T4 blank at the punch stroke of 25mm

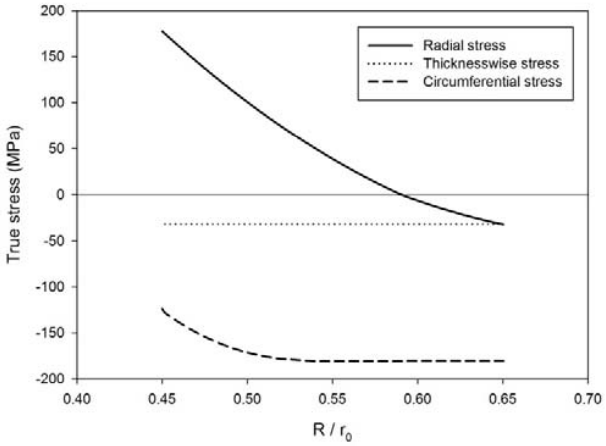

Fig. 11 Stress distribution in AA6061-T4 blank at the punch stroke of 50mm

One of the most important parameters in the analysis of hydroforming deep drawing is the estimation of the maximum punch force to select an appropriate forming machine with suitable capacity. The effect of key process parameters on the maximum necessary drawing force of the hydroforming deep drawing process is investigated using (21). Friction is one of the most important parameters affecting the material flow and drawing force subsequently. Fig. 14 shows the effect of friction between blank and metallic tools on the maximum punch force. As can be seen from the figure, as the coefficient of friction increases, the maximum punch force necessary to perform the deep drawing process increases. The results of FE simulations with different values of friction coefficients are also presented in Fig. 14. It is clear from the figure that, compared with the numerical simulations, (21) is more sensitive to the value of the coefficient of friction and predicts a higher punch force.

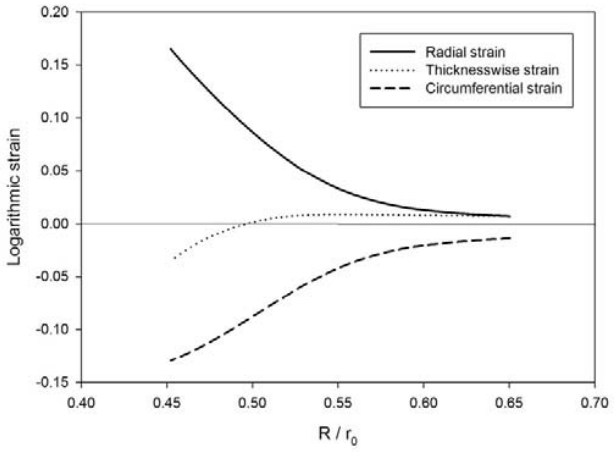

Fig. 12 Logarithmic strain in AA6061-T4 blank at the punch stroke of 50mm

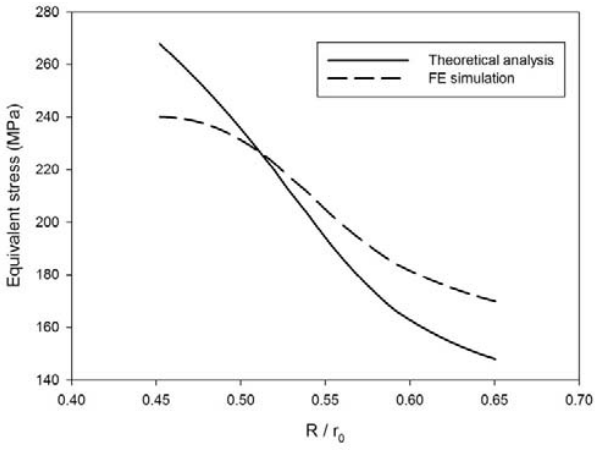

Fig. 13 Comparison of analytical analysis and FE simulation for prediction of equivalent stress

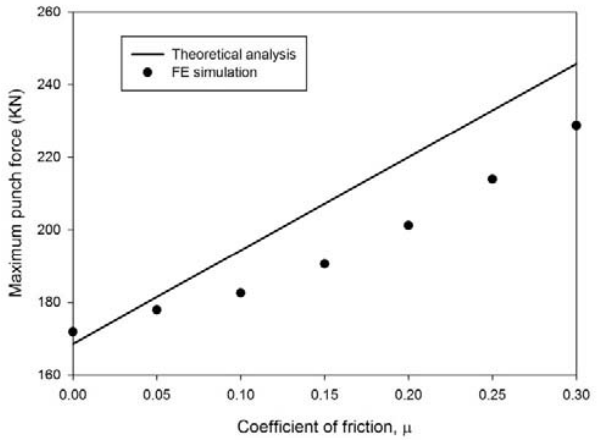

Fig. 14 Effect of friction coefficient on maximum punch force

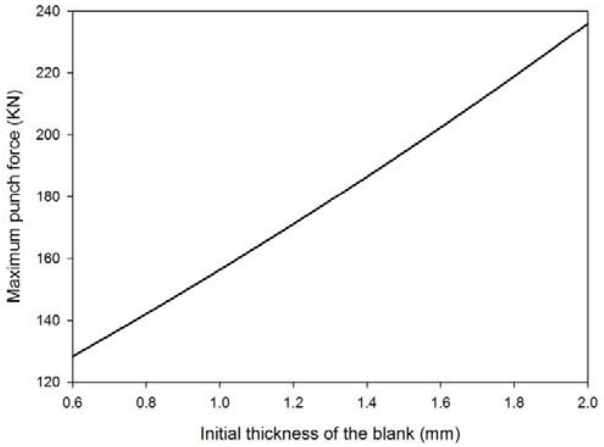

Fig. 15 Effect of blank initial thickness on maximum punch force

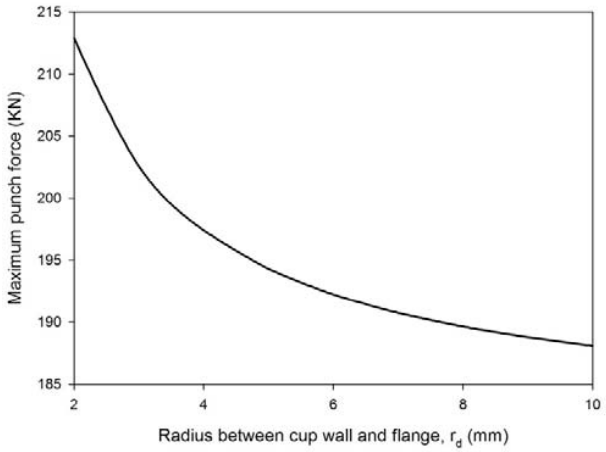

Fig. 16 Effect of bend radius on maximum punch force

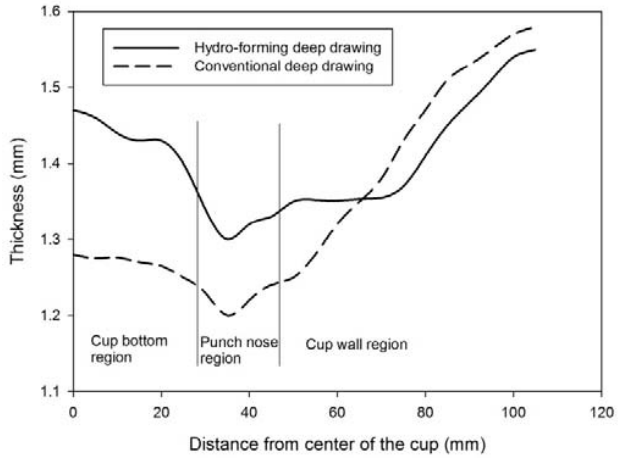

Fig. 17 Variation of thickness of the drawn cup at the end of the process

The effect of the initial thickness of the blank on the maximum punch force is presented in Fig. 15. As can be seen from the figure, as the initial thickness of the blank increases, the necessary load to carry out the process increases. The influence of bending radius r_d, between cup wall and flange on the punch force is also shown in Fig. 16. According to this figure, drawing the cups with a bigger bend radius needs lower press capacity. This is due to the lower stress needed for a bigger bend radius and the lower friction force needed.

Fig. 17 shows the variation of thickness at the drawn cup at the end of the hydroforming deep drawing simulation. As illustrated in the figure, a very small thinning happens in the bottom region. The maximum thinning appears at the punch nose region due to the excessive stretching of the material during the process. Along the cup wall region, thinning happens at the bottom and at the top of the cup, we have thickening. To compare the results of a hydroforming deep drawing with conventional deep drawing process, finite element simulation of conventional deep drawing process has been carried out with the same geometry and forming conditions of hydroforming process. As shown in Fig. 17, the thickness distribution is more uniform for the hydroforming deep drawing process compared with the conventional process. This uniform thickness distribution is one of the significant advantages of the hydroforming deep drawing [2]. The maximum thinning in the drawn cup is 13% using the hydroforming method and 20% using the conventional method. The results show that for conventional deep drawing, maximum thinning occurs in the same area as for the hydroforming process. However the value of thinning in the bottom and punch nose area is bigger than the hydroforming process. It shows that the risk of tearing of the drawn cup can be reduced significantly using the hydroforming method.

V. Conclusions

In this paper the hydroforming deep drawing process was investigated using mathematical models and finite element simulations. The main conclusions of this research are summarized below:

- The deformation mechanism of the cup during the hydroforming deep drawing process is a combination of tensile radial stress and compressive circumferential and thicknesswise stresses.
- The analytical model predicts the maximum punch force with about 6% difference compared to the FE simulation.
- As the coefficient of friction increases, the maximum punch force necessary to perform the deep drawing process increases. Compared with the numerical simulations, the analytical model is more sensitive to the value of coefficient of friction.
- As the initial thickness of the blank increases, the maximum punch force to carry out the hydroforming deep drawing process increases.
- Drawing the cups with a bigger bend radius needs lower press capacity.
- Simulation results show that the risk of tearing of the drawn cup can be reduced significantly using the hydroforming method instead of conventional deep drawing.

References

[1] Thiruvarudchelvan, S. and Travis, F.W. (2003) Hydraulic-pressure-enhanced cup-drawing processes - An appraisal. Journal of Materials Processing Technology 140 (1-3 SPEC.), pp. 70-75.
[2] Ramezani, M. and Ripin, Z.M. (2012) Rubber-pad forming processes: technology and applications. Woodhead Publishing Ltd, ISBN-13: 978-0857090942, UK.
[3] Fukui, S., Yoshida, K. and Abe, K. (1958) Deep drawing of cylindrical shell according to the so-called hydroform method. Japan Aerospace Exploration Agency, Report No. 333, 24(4), 77-98.
[4] Yossifon, S. and Tirosh, J. (1988) On the Permissible Fluid-Pressure Path in Hydroforming Deep Drawing Processes—Analysis of Failures and Experiments. Journal of Engineering for Industry 110 (2), pp. 146-152.
[5] Thiruvarudchelvan, S. and Lewis, W. (1999) Note on hydroforming with constant fluid pressure. Journal of Materials Processing Technology 88 (1), pp. 51-56.
[6] Vollertsen, F., Breede, R. and Lange, K. (1999) Method for deep drawing with multiple elastomer membranes. CIRP Annals - Manufacturing Technology 48 (1), pp. 221-226.

[7] Kandil, A. (2003) An experimental study of hydroforming deep drawing. Journal of Materials Processing Technology 134 (1), pp. 70-80.
[8] Lang, L., Danckert, J. and Nielsen, K.B. (2004) Investigation into hydrodynamic deep drawing assisted by radial pressure: Part I. Experimental observations of the forming process of aluminum alloy. Journal of Materials Processing Technology 148 (1), pp. 119-131.
[9] Lang, L., Danckert, J. and Nielsen, K.B. (2005) Investigation into hydrodynamic deep drawing assisted by radial pressure: Part II. Numerical analysis of the drawing mechanism and the process parameters. Journal of Materials Processing Technology 166 (1), pp. 150-161.
[10] Djavanroodi, F. and Derogar, A. (2010) Experimental and numerical evaluation of forming limit diagram for Ti6Al4V titanium and Al6061-T6 aluminum alloys sheets. Materials and Design 31 (10), pp. 4866-4875.
[11] Chang, D. F. and Wang, J.E. (1998) Analysis of draw-redraw processes. International Journal of Mechanical Sciences 40 (8), pp. 793-804.
[12] Morovvati, M.R., Mollaei-Dariani, B. and Asadian-Ardakani, M.H. (2010) A theoretical, numerical, and experimental investigation of plastic wrinkling of circular two-layer sheet metal in the deep drawing. Journal of Materials Processing Technology 210 (13), pp. 1738-1747.
[13] Mielnik, E.K. (1991) Metalworking Science and Engineering. McGraw-Hill, New York, ISBN: 0-07-041904-3.
[14] Ramezani, M., Ripin, Z.M. and Ahmad, R. (2009) Computer aided modelling of friction in rubber-pad forming process. Journal of Materials Processing Technology 209 (10), pp. 4925-4934.
[15] Ogden, R.W. (1972) Large deformation isotropic elasticity–on the correlation of theory and experiment for incompressible rubberlike solids. Proceedings of the Royal Society of London, Part A 326, pp. 565-84.
[16] Ramezani, M. and Ripin, Z.M. (2010) Combined experimental and numerical analysis of bulge test at high strain rates using split Hopkinson pressure bar apparatus. Journal of Materials Processing Technology 210 (8), pp. 1061-1069.
[17] Panknin, W. and Mulhauser, W. (1957) Principles of the hydroform process, Mitt. Forschung. Blechver. 24, pp. 269-277.